# Microfibril angle of elementary flax fibres investigated with polarised second harmonic generation microscopy

Alessia Melelli, Frédéric Jamme, David Legland, Johnny Beaugrand, Alain Bourmaud

# Microfibril angle of elementary flax fibres investigated with polarised second harmonic generation microscopy

Alessia Melelli[1], Frédéric Jamme[2], David Legland[3],

Johnny Beaugrand[3], Alain Bourmaud[1]

[1] Univ. Bretagne Sud, UMR CNRS 6027, IRDL, Lorient, France

[2] Synchrotron SOLEIL, DISCO beamline, Gif-sur-Yvette, France

[3] UR1268 Biopolymères Interactions Assemblages, INRAE, Nantes, France

Corresponding author: alain.bourmaud@univ-ubs.fr

## ABSTRACT

Over the last decades, bio-based composite materials have been developed as an ecological alternative to synthetic fibre-reinforced composites, and flax fibres are one of the most commonly used fibres for this purpose. The secondary cell wall (S2) and the microfibril angle (MFA) of plant fibres are the main factors responsible for the mechanical behaviour of the fibres and, consequently, for the properties of the final biocomposite material. However, the MFA values reported in the literature are obtained through heavy, time-consuming methods and often without resolution at the scale of the elementary fibres. In the present paper, for the first time, the MFAs of elementary flax fibres are measured with the alternative method of second-harmonic generation imaging under controlled polarised light (P-SHG); cotton trichomes are also investigated as a homogeneous and well-known cellulose fibre with expected contrasted MFAs compared to flax. To estimate the MFA, we analysed the images collected that clearly show the microfibrils. The values found are in line with the literature

data obtained with conventional techniques. However, new important details of the microfibrils orientation of elementary flax fibres and cotton trichomes are highlighted, such as inhomogeneities in a single flax fibre, leading to MFAs varying between 0 and 10° along the fibre with an average value around 5°. The results obtained give an important contribution to the knowledge of the plant fibre ultrastructure, giving some structural details never provided with measurements of fibre bundles.

**Keywords:** SHG**,** Microfibril angle; Elementary fibres; Flax fibres; Image analysis

## 1. INTRODUCTION

Flax fibres have been used for centuries as one of the most important textile materials due to their extraordinary morphology and mechanical properties, but in the last few years, interest in plant fibres has increased as a result of the development of biocomposite materials in which not only resins, such as poly-(hydroxyalkanoate resin) (PHA) and poly-(lactid) (PLA), but also widely industrially used poly-(propylene) (PP) (Bensadoun et al., 2016) are coupled with plant fibres for the automotive, sport and design industries (Deyholos and Potter, 2014; Le Duigou et al., 2014). Flax fibres have high specific mechanical properties as well as low environmental impact in comparison with glass fibres (Lefeuvre et al., 2014a; Joshi et al., 2004) and a clear example of the use of plant fibre composites is for car components, with the advantages of reduced cost and weight of the vehicle (Bledzki et al., 2006).

However, one of the main problems for bio-composite development is the prediction of mechanical behaviour, especially if the fibres are heterogeneous (José da Silva et al., 2012). Mechanical properties of plant fibre change according to several factors, such as the fibre phylogenetic origin or the environmental condition during plant growth, which introduces uncertainties into the prediction of mechanical performance of the finished product. Besides,

some aspects of the plant fibre ultrastructure, the internal structural arrangement of the fibre elements, are still not fully elucidated.

Elementary flax fibre is composed of one long but single multi-nuclei cell (Ageeva et al., 2005). Several fibres, between 10 and 40 units, are grouped in bundles (Baley, 2002) and located in the region of the phloem, with the main role of mechanical support of plants. Single fibres are assembled by middle lamellae, enriched in pectic polysaccharides and linked by covalent and calcium bridge bonds (Jauneau et al., 1992). Figure 1 presents the structure of a single flax fibre. The outer layer of the fibre is the primary cell wall (P) of 0.2 μm thickness, mainly composed of amorphous pectins, hemicellulose and lignin, with the cellulose microfibrils reoriented during the intrusive growth in the cell development (Baley et al., 2018) according to the fibre axis. The inner and main layer is the secondary cell wall, which is mainly composed of crystalline cellulose and can be divided into three sublayers. In the literature, it is known that these sublayers have different cellulose microfibrillar angles (MFA). The S1 layer has a thickness of 0.2-5 μm, and the cellulose microfibrils are crisscrossed (Wang et al., 2018; Baley, 2002; Bos and Donald, 1999) or, as reported in another recent paper, have a Z-twist orientation but with uncertainty in the angle (Baley et al., 2018). The S2 layer is 5-10 μm thick with an MFA of 6°-11° (Wang et al., 2018; Bourmaud et al., 2013; Baley, 2002; Astley and Donald, 2001). Finally, the 0.5-1 μm thick S3 layer surrounds the hollow centre of the fibres called the lumen (Wang et al., 2018).

Figure 1

Cellulose fibrils are cellulose crystallites assembled into longitudinal nanofibres, and hemicellulose and pectin glue several nanofibres together to form a single microfibril with a helical disposition (Duchemin et al., 2012; Wardrop, 1962; Ritter, 1942). The thickness of the layers and the orientation and morphology of the cellulose microfibrils vary between botanical

species, as do the chemical composition and mechanical properties. For example, it is known that cotton trichomes have a microfibril angle of 25-30° in the S2 layer (Ioelovich, 2014; Ansell and Mwaikambo, 2009), which is higher than that of flax. Moreover, the microfibrils in the S2 layer for flax have a diameter between 10 and 20 nm (Baley, 2002), and Ansell and Mwaikambo (2009) reported that the thicknesses of cellulose microfibrils of different origin, for example, cotton or hemp, are of the same order of magnitude as that of flax.

Literature shows that plant fibres used for composite reinforcement exhibit strong differences into their intrinsic characteristics (Netravali, 2005) and structure (Bourmaud et al., 2018). Chemical composition and structure of some varieties of flax were correlated with the mechanical properties (Bourmaud et al., 2013). The results showed a relationship between the MFA and Young's modulus, while it appeared that there is no correlation between the MFA and the strain at break of elementary fibres. Another study on hemp and sisal fibres highlighted the relationship of the MFA with the stress-strain curve, and the authors noted a linear trend for sisal (MFA=20°), while hemp has a less linear behaviour (MFA=10°) (Bourmaud and Baley, 2009). Thus, the MFA is strongly linked to the mechanical properties or behaviour of plant fibres and consequently to those of associated composites.

MFA of wood fibres has been extensively studied from the role inside the plant to the mechanical properties correlated and the environmental impact on their variability (Donaldson, 2008); this holistic review offers a complete overview of MFA investigation methods; some such as the pit method or confocal microscopy are particularly adapted to elementary fibres, but the most popular technique is X-Ray Diffraction (XRD), despite it is mostly limited to fibre bundles. Thus, there is little information about the microfibril angle of bast fibres, particularly at the single fibre scale. In general, if the angle is too small the resolution of the analytical techniques used is often insufficient to evaluate it for an elementary fibre (Bourmaud et al., 2013). Nevertheless, Müller et al. successfully applied micro-small-angle X-ray scattering/wide-angle X-ray diffraction (μSAXS/WAXD) to

elementary flax fibres (Müller et al., 2000; Muller et al., 1998). In Tab. 1, a summary of the MFA values found for flax fibres (measured at room temperature and relative humidity) are reported along with the method used. A more complete table with other methods used to evaluate the microfibril angle of a range of plant fibres can be found in the chapter written by Ansell and Mwaikambo (Ansell & Mwaikambo, 2009). Recently, Wang et al. (Wang et al., 2018) mechanically removed the outer layer of flax fibre bundles to directly investigate the MFA by scanning electron microscopy (SEM) and X-ray diffraction (XRD); they reported MFA values between 5.8 and 7.3°, which is consistent with literature data (Tab.1). They underlined that uncertainties in MFA values may be due not only to the use of fibre bundles but also to an additional signal induced by refraction effects at the fibre edge. Other differences in the MFA of flax were noted between dry and wet fibres and the results showed an increase in the angle when wet fibres were considered (Astley and Donald, 2001; Muller et al., 1998).

Table 1

The development of new tools for material characterisation has provided the possibility of more accurately studying the ultrastructure of plant fibres. This is the case for second-harmonic generation (SHG) imaging, which can be considered a new tool for accurately investigating the orientation of the microfibrils. Second-harmonic generation is a coherent non-linear optical process in which two lower-energy photons interacting with a medium are up-converted to a single photon with twice the incident frequency (2ω) (Boyd, 2008; Gauderon et al., 2001). The SHG signal is generated from non-centrosymmetric structures and is dependent on many factors, including the polarisation of the light used for imaging and the structural organisation of the sample. One of the main advantages of this technique is the use of low energy excitation, which reduces the beam damage and photobleaching of the sample (Cox and Kable, 2006).

In the last decade, SHG imaging has emerged as a powerful tool in biology, where it has been applied to the study of collagen and in vivo samples (Thomas et al., 2017; Zubkovs et al., 2014; Cox and Kable, 2006; Williams et al., 2005). In particular, in the study of rat-tendon fascicles, Goulam Housen et al. (Goulam Houssen et al., 2011) concluded that a reconfiguration of the collagen microstructure occurs after mechanical tests (uniaxial tensile tests.

In plant research, some aspects have been already investigated using the second-harmonic generation imaging. Cellulose is a non-centrosymmetric molecule and has the potential to produce SHG signal. Cellulose from two different organisms, the Acetobacter xylinum and the Valonia algae, can be detected thanks to the high SHG intensity due to the cellulose molecules that are chiral and well-ordered (Brown, Jr. et al., 2003). The same team also used the light polarization control to investigate the dependence of the signal response of the cellulose microfibrils to the laser orientation and showed that this response is not linear, as expected from the nature of the SHG signal.

More recently, cell walls of both root and leaf sorghum were investigated with the second-harmonic generation imaging microscopy and the authors found a strong signal that they attributed to the cellulose microfibrils of the plant cell wall (Heiner et al., 2018). Therefore, the specific structure and arrangement of cellulose within flax cell walls (Fig.1) fully justify the use of SHG for MFA investigations. Cox et al. investigated several samples like stem from living plants (Lantana camara) but also rice starch grains of different varieties. The authors showed how starch generates a higher SHG signal if compared with cellulose due to a lower symmetry of the glucose chain (Cox et al., 2005). Zhao et al. also used SHG microscopy to map the sugar and amylopectin distribution in glutinous and non-glutinous rice grains. They found differences between the two varieties due to the SHG responses (Zhao et al., 2018). Amylopectins are responsible for the SHG signals due to the crystallites arranged in a double helix structure (Nessi et al., 2018) and a calibration method to define the SHG signal at each

laser polarization angle in the P-SHG technique had been developed with the use of starch granules (Mazumder et al., 2013; Psilodimitrakopoulos et al., 2008).

The objective of the present work is to estimate the MFA of single flax fibres using, unprecedented in the literature, a novel approach offered by the potential of SHG measurements. Detailed results are shown for flax fibres; besides, cotton trichomes were analysed due to the contrasted value of their MFA, which makes them clearly distinguishable from flax. The method is a direct measurement of the MFA from an image of the cellulose microfibrils and showed various heterogeneities of MFA that could be related to mechanical properties of the fibres.

## 2. MATERIALS AND METHODS

### 2.1. Materials

Elementary flax fibres were extracted from a batch of the Bolchoï variety (year 2018, classification number 66233) cultivated in Normandy by the Depestele group. After growth, flax fibres were pulled out, dew retted for 6 weeks and mechanically scutched. The diameter of each flax fibre was approximately 20 µm. Raw flax fibres are shown in Figure 2.a.

Figure 2

Besides, cotton trichomes were investigated to increase the range of MFA measurements and validate the method. The cotton trichomes were issued from G3 BRS 293 and were cultivated in Ntarla, Mali, in 2017.

Each fibre was directly mounted on a 150 µm thick paper support, commonly used for single fibre tensile tests (as reported in Figure 2 a) and the sample was placed between two coverslips to improve the observations and tuning of the microscope. Fig. 2.b shows a single

183 flax fibre glued on a paper support commonly used for tensile tests according to ASTM
184 C1557.

185

186

187 **2.2. Methods**

188 A multiphoton Nikon A1 MP+ microscope (NIKON, France) equipped with a long working
189 distance 16x water immersion objective (NA 0.80, NIKON, France) was used for the
190 acquisition, and a half-wave plate (HWP) (MKS-Newport, USA) was rotated to control the
191 laser polarisation angle. Figure 2.c shows the SHG microscope.

192 The femtosecond laser used was a tuneable Mai Tai XF mode-locked Ti:sapphire
193 femtosecond laser (SPECTRA PHYSICS, France), and an excitation wavelength of 810 nm
194 was chosen (the average power is 1.5 W at 810 nm.) The maximum laser power percentage
195 used was 10%. The channels used were both the autofluorescence collected at 460/60 and
196 550/88 nm and SHG signals (forward and backward signals collected at 406/15 nm) detected
197 by GaAsP NDD (gallium arsenide non-descanned) detectors. The scan line average was 8,
198 the scan velocity was fixed at 1 (fps) and the scan size was 512*512 pixels.

199 All the measurements were performed at room temperature; Fig. 3 illustrates the optical
200 configuration of the multiphoton microscope.

201

202 Figure 3

203

204 The first acquisitions were performed on flax fibres to establish the maximum of the average
205 excitation laser power (before laser beam damage). An average laser power percentage of
206 10% max was used for the firsts acquisitions. However, damage due to the laser power was
207 observed if the fibre had some thermolabile middle lamella pectic remnants on the surface in

the case of under-retted fibres or the presence of small damages due to fibre extraction. Thus, to avoid any damage, the laser power was successively set at 5%.

To evaluate the microfibril angle, the half wave plate (HWP) was rotated to estimate the range of angles with the maximum intensity of the second-harmonic generation emitted for each flax fibre and cotton trichome. Subsequently, as SHG allows optical sectioning, the signal was optimized to select the depth of the fibre that showed the maximum intensity, and finally, an image was collected at the rotation angle that better highlighted the pattern of the cellulose microfibrils.

The four images collected at different polarisation angles illustrate a flax fibre with a starch granule of spherical shape deposited on the surface (Fig. 4). By changing the HWP rotation angle, it is possible to identify the range of angles where the plant fibre has the maximum SHG emission.

Figure 4

A maize starch grain can generate a second-harmonic signal at each angle of the HWP (Psilodimitrakopoulos et al., 2008). Thus, we can compare the SHG signal of a maize starch grain with the SHG signal of fibres and trichomes as reported in Fig.4. An image sequence was collected at each rotation angle, and the image of the starch grain at the same polarisation angle as the maximum SHG signal of the fibre was chosen. The maximum SHG intensities of the starch grain were identified, and the angle measured corresponds to the angle of the cellulose microfibrils inside the fibre.

The software used for the imaging acquisition was NIS elements (NIKON, France), and the software used for the image processing was ImageJ (National Institute of Health, USA) (Schneider et al., 2012).

To evaluate the microfibril angle, a MATLAB script has been written to identify and calculate the angles of microfibrils and create histograms of their frequency. The microfibril angle was evaluated by an image analysis procedure that computed the histogram of the preferred orientation of pixels, using an approach developed in Gager et al. (Gager et al., 2020). Briefly, the preferred orientation is computed by (1) applying grey-level granulometry curves with various orientations, (2) computing a typical size in each direction, (3) and estimating the preferred orientation from typical sizes. Grey-level granulometry is an approach for image texture analysis based on the application of morphological operators (typically opening or closing) using a family of structuring elements of increasing size (Fig.5-A to 5-H) (Devaux and Legland, 2014; Devaux et al., 2008; Soille, 2004). Measuring the differences in grey levels of images after each opening or closing step results in a granulometry curve that depicts the size distribution of the structures within the image.

Figure 5

Granulometry curve computed for the whole image can be summarised by a grey-level mean size corresponding to the typical size of the structures within the image. The grey level mean size can also be computed for each pixel to investigate the typical size of the structure it belongs to, resulting in a local granulometry (Soille, 2004, 2002). In order to assess the preferred orientation of the microfibrils, linear structuring elements with orientations ranging from 0 to 180 degrees were used (Devaux and Legland, 2014; Legland et al., 2012; Devaux et al., 2008; Soille, 2002). The computation of granulometry curves for each orientation results in a function that depicts the typical size of each pixel depending on the orientation (Fig. 5-I and 5-J). For pixels belonging to a microfibril, this function presents a peak for the angle corresponding to the microfibril orientation (Fig. 5-K). The preferred orientation of each pixel is estimated by integrating the typical size function over the range (0, 180) degrees, and

259 represented using a colour code that considers both the orientation and the intensity of the
260 pixel (Fig. 5-L). Finally, the distribution of the microfibril angles is obtained by computing the
261 histogram of the preferred orientation of the microfibril pixels.

262

263 ## 3. RESULTS AND DISCUSSIONS

264 The SHG emitted in the forward direction is higher than the SHG emitted in the backward
265 direction due to the coherent nature of the process, but backward SHG can give
266 complementary information; especially when the sample is thick, the backward direction is
267 the only possible way to investigate (Pavone and Campagnola, 2013; Cox and Kable, 2006).
268 The difference between backward and forward images from Valonia algae, which highlight
269 differences in cellulose microfibrils, was already reported in (Nadiarnykh et al., 2007). In our
270 case, flax fibres and cotton trichomes show both high SHG signal intensities in the forward
271 direction and therefore we select it (Fig.6).

272 In the images acquired, cellulose microfibrils present a characteristic pattern perpendicular to
273 the microfibril length with alternating bands due to their highly ordered arrangement. A similar
274 pattern was observed for nematode muscle by Campagnola et al. (Campagnola et al., 2002).
275 The authors reported that the lower limit for harmonic emission from the electric dipole
276 interaction is λ/10; for a smaller distance, the asymmetric condition is broken, and SHG
277 emission does not occur.

278

279 Figure 6

280

281 Nevertheless, due to the MFA orientation, cellulose microfibrils are visible only over a
282 specific range of the HWP rotation angle, and to identify this range, it is necessary to
283 investigate flax fibres and trichomes at each polarisation angle using the P-SHG technique.

As expected, we found between 2°-3° for flax and around 25°-26° for cotton microfibrils. The microfibrils are well distinguishable, and it is possible to acquire images and precisely measure the orientation taking the fibre axis as the reference X-axis. In Fig.7, the visible patterns of microfibrils of flax and cotton are shown.

Figure 7

Besides, a range of elementary flax fibres was investigated, and even when their MFAs have a preferential orientation in agreement with the literature (Bourmaud et al., 2013; Astley and Donald, 2001; Muller et al., 1998), we observed that the microfibril orientation changes according to the considered area. This is particularly evident in flax fibre investigated in Fig.8 where the MFA is close to 5° in some specific spots while in others it is almost parallel to the fibre axis (0°).

This is a clear advantage of the SHG microscopic imaging technique where local areas of single elementary fibres can be analysed, oppositely to XRD, for example.

In Fig.9 the same image reported in Fig.8b was processed thanks to a MATLAB script specifically created with the purpose of estimating the local orientation of microfibrils and computing the histogram of the orientations.

Figure 8

The whole image has been processed as well as the three sections separately, and slight heterogeneities in the orientation of microfibrils can be revealed. Ninety percent of the values measured are less than 10° to the fibre axis (Fig 9-A) and the mean value over the whole area is 5.3 ± 3.3°. Interestingly, the histograms highlight differences between zones with a

309 progressive diminution of the microfibril angle (Fig. 9 E, F) near a dislocation (kink-band) that
310 is present along the fibre (Fig.9-B, grey arrow).

311

312 Figure 9

313

314 Under these observations, it is difficult to establish a single microfibril angle for a single
315 elementary fibre and, consequently, for a fibre variety, as is often reported in the literature.

316 This diversity in the organisation of cellulose cannot be determined by averaged
317 measurements, as is the case with X-ray diffraction, for example; it is therefore rarely
318 discussed in the literature. For example, for flax fibres, it has been shown by TEM analysis
319 (Roland et al., 1995) that transition zones of angles exist, which also supports the hypothesis
320 of misalignments such as those shown here. Thus, the relatively small angle value that we
321 highlight here, compared to the data in the literature (Tab.1), takes on its full meaning when it
322 is related to the inherent nature of flax walls.

323 The low values of microfibrillary angles found here, as well as their dispersion, are
324 particularly important data, especially for the biocomposite community when fibres are used
325 as reinforcements. Indeed, fibre stiffness and Young's modulus are inversely correlated with
326 MFA (Bourmaud et al., 2013), also demonstrated by wood community using nanoindentation
327 (Eder et al., 2013; Jäger et al., 2011). Our results now make it possible to envisage a more
328 detailed exploration of the evolution of MFA, whether it is a function of the varieties studied,
329 but also of growing conditions, environmental stress and fibre extraction or processing
330 conditions as in wood (Donaldson, 2008). Finally, during a tensile test on elementary fibre, it
331 was shown that MFA decreases, the first part of the tensile stress being marked by a
332 reorientation of the cellulose macro fibrils (Lefeuvre et al., 2014b). This phenomenon results
333 in a non-linearity at the beginning of the stress-strain curve, which represents a strong
334 signature of single plant fibres mechanical behaviour.

For cotton trichomes, by changing the polarisation angle, it was also found that two different and opposite orientations (right-handed Z and left-handed S helix, respectively) of the microfibrils are present, forming a criss-cross pattern (see Fig. 10a and the structure schematised in Fig. 10b). The sample plane in the Z direction (depth of the trichome) is the same, but because the cotton trichomes are twisted (Dochia et al., 2012), different layers can be involved, and their interpretation become more difficult.

Figure 10

Other interesting information can be found by scanning at different Z values as second-harmonic microscopy is plane selective and allows the analysis of a single level without or with little interference from the other levels (Brown, Jr. et al., 2003). Fig.11 shows that fibres are surrounded by an external layer on the edges, identified as the primary cell wall (P) and the S1 layer. The lumen in the middle (L) is delimited by the S3 layer that makes it visible. The lumen is visible only at a specific depth of the fibre. Interestingly, a fluorescent signal is observed at the edge of the lumen, helping in focusing and discerning this hollow structure. The origin of this fluorescence is arguably the vestiges of cytosolic fluorescent components left at the surface of the apoplasm through fibre senescence or apoptosis. Indeed, in such multinucleate fibres, it is likely that membrane-bound “apoptotic bodies” formed (Evert, 2006), were engulfed and more or less degraded into nucleic acid. Additionally, fluorescence signals can be from mitochondria, which are well known to liberate many fluorescent cytochrome components after programmed cell death (Skulachev et al., 2009).

Figure 11

360 The combination of the two SHG channels (forward and backward signals) does not show
361 these details, and an autofluorescence signal is needed to highlight them. Indeed, in plant
362 cell walls, suberin, lignin, cutin and a small number of proteins produce autofluorescence
363 emission, as reported by Berg (Berg, 2004). Day et al. measured the lignin inside the
364 different layers of flax bast fibre cell walls and found GS lignin in the secondary cell wall as
365 well as a significant amount of condensed G lignin in the S1 layer together with the other two
366 GS epitopes (Day et al., 2005).

367 Microfibrils are also present in the P and S1 layers (Fig. 1), but they cannot be detected and
368 correctly visualised due to their small thicknesses.

369 Regarding the lumen, flax fibre cell walls change their structure during growth. In a not fully
370 developed flax fibre, two types of layers have been identified: the G (S2) layer, which is the
371 mature part of the cell wall, and the Gn (S3) layer, which is the newly deposited layer of the
372 gelatinous cell wall (Goudenhooft et al., 2018). The Gn layer is deposited from the outer to
373 the inner side of the cell, and with maturation, the Gn layer changes its cell wall density and
374 non-cellulosic polymer arrangement, becoming a mature G layer; these two layers mainly
375 differ in the length of galactan chains, as reported by Rihouey et al. (Rihouey et al., 2017).
376 Thus, the more mature the fibre is, the smaller the lumen, and its diameter varies between
377 fibres. The size of the lumen may also depend on environmental conditions. In the case of
378 low temperature or the lodging phenomenon, conversion of Gn into the G layer may be
379 stopped, inducing a large lumen. Nevertheless, even for a fully developed fibre, a small part
380 of the S3 layer is still present. Regarding both the macromolecules and the small size
381 molecules that compose the cell wall, they are undoubtedly heterogeneously distributed over
382 the layers described earlier (Bourmaud et al., 2018). In line with the scope of this paper,
383 phenolic structures are present in these layers, and with the particular G-rich lignin quantified
384 and immunolocalised across flax fibres (Day et al., 2005), these structures arguably emit
385 fluorescence detectable at approximately 550 nm (pink). The literature also reported small
386 molecules based on solid-state 13C NMR (Love et al., 1994), namely, anthocyanins and

387 ferulates (hydroxycinnamics), which are supposed to emit a detectable fluorescence signal,
388 for instance, a blue signal at approximately 460 nm.
389

390 This method has several important advantages: several areas of the same fibre can be
391 investigated, so the variation in the microfibril organisation can be highlighted; and the MFA
392 is measured and not estimated, it is possible to change the environment and collect images
393 to estimate the modification in the structure.

394 In a future work, the inhomogeneities in elementary flax fibres, such as kink bands, will be
395 investigated to deeply explore their specific ultrastructure and local arrangement of cellulose
396 microfibrils and, in addition, several mediums and environments will be tested (immersion in
397 various media etc.) to better understand the structure of the single fibres and its modification.

398

## 399 4. CONCLUSION

400 To date, researchers have used several techniques to evaluate the microfibril angle, such as
401 X-ray diffraction (XRD), scanning electron microscopy (SEM) and microbeam small-angle X-
402 ray scattering (μSAXS), but each of these techniques has some disadvantages.

403 In this work, the MFAs of elementary flax fibres and cotton trichomes were successfully
404 calculated for the first time using second-harmonic microscopy under controlled polarisation
405 light (P-SHG). The MFAs of flax and cotton were calculated using a direct evaluation of the
406 microfibril angle observed in P-SHG images.

407 In fact, the resolution of this technique is such that macrofibrils are visible in the images
408 collected, and their angles can be directly measured. This method not only allows us to
409 obtain precise angles of the cellulose macrofibrils, when other techniques can only measure
410 an average (confirming, however, the preferential orientations between 2° and 7° for flax
411 fibres and approximately 26° for cotton trichomes already reported in the literature), but also
412 allows us to investigate a length of several tens of micrometres for a single elementary fibre.

In light of these new results, it is clear that the microfibril organisation in a fibre is inhomogeneous, depends on the zone analysed and can have an orientation parallel to the axis of the flax fibre or a specific angle. This fact can also explain the large range of values found by other research teams, regardless of the methodology used.

Several planes in the Z-axis can also be analysed, and the second-harmonic emission for each position can be evaluated to compare the behaviour of the whole fibre. A limit we face is the need for non-twisted fibre elements, and our cotton trichome, taken as a reference, illustrates this with its numerous twists. However, if the whole length of the fibre elements cannot be observed, then a limited area is enough for the SHG measurement.

In conclusion, in this paper, new important information on the ultrastructure of plant fibres is presented, and P-SHG demonstrates high potential for studying the variation in the MFA under different environmental conditions and at local defects, i.e., few µm kink bands, owing to its high resolution. Future work will focus on evaluating the inhomogeneities of the microfibril organisation and, more specifically, the specific ultrastructure in critical areas, such as kink bands and structural defects. Several environmental conditions will also be tested to investigate the reorganisation of the microfibrils, as well as possible MFA variation into the thickness of the fibre thanks to z-stack explorations.

## ACKNOWLEDGEMENTS

The authors want to thank the INTERREG IV Cross Channel programme for funding this work through the FLOWER project (Grant Number 23). SOLEIL Synchrotron is also thanked for funding the 99180266 in-house proposal, as are Awa Doumbia (CERFITEX, Mali) and Jean-Paul Laclau and Eve Denonnin (CIRAD, Montpellier) for providing cotton trichome samples.

## REFERENCES


Ageeva, M. V, Petrovská, B., Kieft, H., Sal'nikov, V. V, Snegireva, A. V, Dam, J.E.G., Veenendaal, W.L.H., Emons, A.M.C., Gorshkova, T.A., Lammeren, A.A.M., 2005. Intrusive growth of flax phloem fibers is of intercalary type. Planta 222, 565–574. https://doi.org/10.1007/s00425-005-1536-2

Ansell, M.P., Mwaikambo, L.Y., 2009. 2 – The structure of cotton and other plant fibres, in: Handb. of Text. Fibre Struct. pp. 62–94. https://doi.org/10.1533/9781845697310.1.62

Astley, O.M., Donald, A.M., 2001. A Small-Angle X-ray Scattering Study of the Effect of Hydration on the Microstructure of Flax Fibers. Biomacromol. 2, 672–680.

Baley, C., 2002. Analysis of the flax fibres tensile behaviour and analysis of the tensile stiffness increase. Compos. Part A: Appl. Sci. Manuf. 33, 939–948.

Baley, C., Goudenhooft, C., Gibaud, M., Bourmaud, A., 2018. Flax stems: from a specific architecture to an instructive model for bioinspired composite structures. Bioinspir. Biomim. 13, 026007. https://doi.org/10.1088/1748-3190/aaa6b7

Bensadoun, F., Vanderfeesten, B., Verpoest, I., Van Vuure, A.W., Van Acker, K., 2016. Environmental impact assessment of end of life options for flax-MAPP composites. Ind. Crops Prod. 94, 327–341. https://doi.org/10.1016/j.indcrop.2016.09.006

Berg, R.H., 2004. Evaluation of spectral imaging for plant cell analysis. J.Microsc. 214, 174–181. https://doi.org/10.1111/j.0022-2720.2004.01347.x

Bledzki, A.K., Faruk, O., Sperber, V.E., 2006. Cars from Bio-Fibres. Macromol. Mater. Eng. 291, 449–457. https://doi.org/10.1002/mame.200600113

Bos, H.L., Donald, A.M., 1999. In situ ESEM study of the deformation of elementary flax fibres. J. Mater. Sci. 34, 3029–3034.

Bourmaud, A., Baley, C., 2009. Rigidity analysis of polypropylene/vegetal fibre composites after recycling. Polym. Degrad. Stabil. 94, 297–305. https://doi.org/10.1016/j.polymdegradstab.2008.12.010

Bourmaud, A., Beaugrand, J., Shah, D.U., Placet, V., Baley, C., 2018. Towards the design of high-performance plant fibre composites. Prog. Mater. Sci. 97, 347–408.

Bourmaud, A., Morvan, C., Bouali, A., Placet, V., Perré, P., Baley, C., 2013. Relationships between micro-fibrillar angle, mechanical properties and biochemical composition of flax fibers. Ind. Crops Prod. 44, 343–351. http://dx.doi.org/10.1016/j.indcrop.2012.11.031

Boyd, R.W., 2008. Chapter 1: The Nonlinear Optical Susceptibility, in: Nonlinear Opt. Elsevier.

Brown, Jr., R.M., Millard, A.C., Campagnola, P.J., 2003. Macromolecular structure of cellulose studied by second-harmonic generation imaging microscopy. Opt. Lett. 28, 2207. https://doi.org/10.1364/OL.28.002207

Campagnola, P.J., Millard, A.C., Terasaki, M., Hoppe, P.E., Malone, C.J., Mohler, W.A., 2002. Three-Dimensional High-Resolution Second-Harmonic Generation Imaging of Endogenous Structural Proteins in Biological Tissues. Biophys. J. 82, 493–508. https://doi.org/10.1016/S0006-3495(02)75414-3

Cox, G., Kable, E., 2006. Second-Harmonic Imaging of Collagen, in: Taatjes, D.J., Mossman, B.T. (Eds.), Cell Imaging Techniques: Methods and Protocols, Methods in Molecular Biology. Humana Press, Totowa, NJ, pp. 15–35. https://doi.org/10.1007/978-1-59259-993-6_2

Cox, G., Moreno, N., Feijó, J., 2005. Second-harmonic imaging of plant polysaccharides. J. Biomed. Opt. 10, 024013. https://doi.org/10.1117/1.1896005

Day, A., Ruel, K., Neutelings, G., Crônier, D., David, H., Hawkins, S., Chabbert, B., 2005. Lignification in the flax stem: Evidence for an unusual lignin in bast fibers. Planta 222, 234–245. https://doi.org/10.1007/s00425-005-1537-1

Devaux, M.F., Bouchet, B., Legland, D., Guillon, F., Lahaye, M., 2008. Macro-vision and grey level granulometry for quantification of tomato pericarp structure. Postharvest Biol. Tec. 47, 199–209. https://doi.org/10.1016/j.postharvbio.2007.06.017

Devaux, M.-F., Legland, D., 2014. Grey level granulometry for histological image analysis of plant tissues, in: Microscopy. Adv. Sci. Res. Educ. pp. 681–688.

Deyholos, M.K., Potter, S., 2014. Engineering bast fiber feedstocks for use in composite materials. Biocatal. Agric. Biotechnol. 3, 53–57. https://doi.org/10.1016/j.bcab.2013.09.001

Dochia, M., Sirghie, C., Kozłowski, R.M., Roskwitalski, Z., 2012. Cotton fibres, in: Handb. of Nat. Fibres. Elsevier, pp. 11–23.

Donaldson, L., 2008. Microfibril Angle: Measurement, Variation and Relationships – A Review. IAWA J. 29, 345–386. https://doi.org/10.1163/22941932-90000192

Duchemin, B., Thuault, A., Vicente, A., Rigaud, B., Fernandez, C., Eve, S., 2012. Ultrastructure of cellulose crystallites in flax textile fibres. Cellul. 19, 1837–1854. https://doi.org/10.1007/s10570-012-9786-1

Eder, M., Arnould, O., Dunlop, J.W.C., Hornatowska, J., Salmen, L., Salmén, L., Salmen, L., 2013. Experimental micromechanical characterisation of wood cell walls. Wood Sci. Technol. 47, 163–182. https://doi.org/10.1007/s00226-012-0515-6

Evert, R.Franklin., 2006. Esau's Plant Anatomy:Meristems, Cells, and Tissues of the Plant Body: Their Structure, Function, and Development. Wiley-Interscience.

Gager, V., Legland, D., Bourmaud, A., Le Duigou, A., Pierre, F., Behlouli, K., Baley, C., 2020. Oriented granulometry to quantify fibre orientation distributions in synthetic and plant fibre composite preforms. Ind. Crops Prod. 151, 112548. https://doi.org/10.1016/j.indcrop.2020.112548

Gauderon, R., Lukins, P.B., Sheppard, C.J.R., 2001. Optimization of second-harmonic generation microscopy. Micron 32, 691–700. https://doi.org/10.1016/S0968-4328(00)00066-4

Goudenhooft, C., Siniscalco, D., Arnould, O., Bourmaud, A., Sire, O., Gorshkova, T.A., Baley, C., 2018. Investigation of the Mechanical Properties of Flax Cell Walls during Plant Development: The Relation between Performance and Cell Wall Structure. Fibers 6, 6. http://dx.doi.org/10.3390/fib6010006

Goulam Houssen, Y., Gusachenko, I., Schanne-Klein, M.-C., Allain, J.-M., 2011. Monitoring micrometer-scale collagen organization in rat-tail tendon upon mechanical strain using second harmonic microscopy. J. Biomech. 44, 2047–2052. https://doi.org/10.1016/j.jbiomech.2011.05.009

Heiner, Z., Zeise, I., Elbaum, R., Kneipp, J., 2018. Insight into plant cell wall chemistry and structure by combination of multiphoton microscopy with Raman imaging. J. Biophotonics 11, e201700164. https://doi.org/10.1002/jbio.201700164

Ioelovich, M., 2014. Cellulose: nanostructured natural polymer. LAP LAMBERT Academic Publishing.

Jäger, A., Hofstetter, K., Buksnowitz, C., Gindl-Altmutter, W., Konnerth, J., 2011. Identification of stiffness tensor components of wood cell walls by means of nanoindentation. Compos. Part A: Appl. Sci. Manuf. 42, 2101–2109. http://dx.doi.org/10.1016/j.compositesa.2011.09.020

Jauneau, A., Morvan, C., Lefebvre, F., Demarty, M., Ripoll, C., Thellier, M., 1992. Differential extractability of calcium and pectic substances in different wall regions of epicotyl cells in young flax plants. J. of Histochem. and Cytochem. 40, 1183–1189.

José da Silva, L., Hallak Panzera, T., Luis Christoforo, A., Miguel Pereira Dur, L., Antonio Rocco Lahr, F., 2012. Numerical and Experimental Analyses of Biocomposites Reinforced with Natural Fibres. IJME 2, 43–49. https://doi.org/10.5923/j.ijme.20120204.03

Joshi, S. V, Drzal, L.T., Mohanty, A.K., Arora, S., 2004. Are natural fiber composites environmentally superior to glass fiber reinforced composites? Compos. Part A: Appl. Sci. Manuf. 35, 371–376.

Le Duigou, A., Bourmaud, A., Davies, P., Baley, C., 2014. Long term immersion in natural seawater of Flax/PLA biocomposite. Ocean Eng. 90, 140–148. https://doi.org/10.1016/j.oceaneng.2014.07.021

538 Lefeuvre, A., Bourmaud, A., Morvan, C., Baley, C., 2014a. Tensile properties of elementary fibres of
539 flax and glass: Analysis of reproducibility and scattering. Mater. Lett. 130, 289–291.
540 http://dx.doi.org/10.1016/j.matlet.2014.05.115
541 Lefeuvre, A., Bourmaud, A., Morvan, C., Baley, C., 2014b. Elementary flax fibre tensile properties:
542 correlation between stress-strain behaviour and fibre composition. Ind. Crops Prod. 52, 762–
543 769. http://dx.doi.org/10.1016/j.indcrop.2013.11.043
544 Legland, D., Devaux, M.-F., Bouchet, B., Guillon, F., Lahaye, M., 2012. Cartography of cell morphology
545 in tomato pericarp at the fruit scale. J. Microsc. 247, 78–93. https://doi.org/10.1111/j.1365-
546 2818.2012.03623.x
547 Love, G.D., Snape, C.E., Jarvis, M.C., Morrison, I.M., 1994. Determination of phenolic structures in flax
548 fibre by solid-state 13C NMR. Phytochem. 35, 489–491. https://doi.org/10.1016/S0031-
549 9422(00)94788-5
550 Mazumder, N., Qiu, J., Foreman, M.R., Romero, C.M., Török, P., Kao, F.-J., 2013. Stokes vector based
551 polarization resolved second harmonic microscopy of starch granules. Biomed. Opt. Express
552 4, 538. https://doi.org/10.1364/BOE.4.000538
553 Müller, M., Czihak, C., Burghammer, M., Riekel, C., 2000. Combined X-ray microbeam small-angle
554 scattering and fibre diffraction experiments on single native cellulose fibres. J. Appl.
555 Crystallogr. 33, 817–819. https://doi.org/10.1107/S0021889800099751
556 Muller, M., Czihak, C., Vogl, G., Fratzl, P., Schober, H., Riekel, C., 1998. Direct Observation of
557 Microfibril Arrangement in a Single Native Cellulose Fiber by Microbeam Small-Angle X-ray
558 Scattering. Macromol. 31, 3953–3957.
559 Nadiarnykh, O., LaComb, R.B., Campagnola, P.J., Mohler, W.A., 2007. Coherent and incoherent SHG
560 in fibrillar cellulose matrices. Opt. Express 15, 3348. https://doi.org/10.1364/OE.15.003348
561 Nessi, V., Rolland-Sabaté, A., Lourdin, D., Jamme, F., Chevigny, C., Kansou, K., 2018. Multi-scale
562 characterization of thermoplastic starch structure using Second Harmonic Generation
563 imaging and NMR. Carbohyd. Polym. 194, 80–88.
564 https://doi.org/10.1016/j.carbpol.2018.04.030
565 Netravali, A.N., 2005. 9 - Biodegradable natural fiber composites, in: Biodeg. and Sustain. Fibres.
566 Woodhead Publishing, pp. 271–309.
567 Pavone, F.S., Campagnola, P.J. (Eds.), 2013. Second Harmonic Generation Imaging, 1 edition. ed. CRC
568 Press, Boca Raton.
569 Psilodimitrakopoulos, S., Amat-Roldan, I., Santos, S., Mathew, M., Thayil K. N., A., Zalvidea, D.,
570 Artigas, D., Loza-Alvarez, P., 2008. Starch granules as a probe for the polarization at the
571 sample plane of a high resolution multiphoton microscope, in: Periasamy, A., So, P.T.C. (Eds.),
572 presented at the Biomedical Optics (BiOS) 2008, San Jose, CA, p. 68600E.
573 https://doi.org/10.1117/12.763168
574 Rihouey, C., Paynel, F., Gorshkova, T., Morvan, C., 2017. Flax fibers: assessing the non-cellulosic
575 polysaccharides and an approach to supramolecular design of the cell wall. Cellul., 24, 1985–
576 2001. https://doi.org/DOI: 10.1007/s10570-017-1246-5
577 Ritter, G.J., 1942. The microstructure of cellulose fibers (No. No.R1432). US Dep. of Agric. Forest
578 Service, Forest Prod. Lab., Madison, Wisconsin.
579 Roland, J.C., Mosiniak, M., Roland, D., 1995. Dynamique du positionnement de la cellulose dans les
580 parois des fibres textiles du lin (Linum usitatissimum). Acta Bot. Gall. 142, 463–484.
581 Schneider, C.A., Rasband, W.S., Eliceiri, K.W., 2012. NIH Image to ImageJ: 25 years of image analysis.
582 Nat. Methods 9, 671–675.
583 Skulachev, V.P., Anisimov, V.N., Antonenko, Y.N., Bakeeva, L.E., Chernyak, B. V, Erichev, V.P., Filenko,
584 O.F., Kalinina, N.I., Kapelko, V.I., Kolosova, N.G., Kopnin, B.P., Korshunova, G.A., Lichinitser,
585 M.R., Obukhova, L.A., Pasyukova, E.G., Pisarenko, O.I., Roginsky, V.A., Ruuge, E.K., Senin, I.I.,
586 Severina, I.I., Skulachev, M. V, Spivak, I.M., Tashlitsky, V.N., Tkachuk, V.A., Vyssokikh, M.Yu.,
587 Yaguzhinsky, L.S., Zorov, D.B., 2009. An attempt to prevent senescence: A mitochondrial
588 approach. Biochim. Biophys. Acta (BBA) - Bioenerg. 1787, 437–461.
589 https://doi.org/10.1016/j.bbabio.2008.12.008

590 Soille, P., 2004. Morphological Image Analysis: Principles and Applications, 2nd ed. Springer-Verlag,
591 Berlin Heidelberg. https://doi.org/10.1007/978-3-662-05088-0
592 Soille, P. (Ed.), 2002. Morphological Texture Analysis: An Introduction, in: Morphology of Condensed
593 Matter: Physics and Geometry of Spatially Complex Systems, Lecture Notes in Physics.
594 Springer-Verlag, Berlin Heidelberg, pp. 215–237. https://doi.org/10.1007/3-540-45782-8
595 Thomas, B., McIntosh, D., Fildes, T., Smith, L., Hargrave, F., Islam, M., Thompson, T., Layfield, R.,
596 Scott, D., Shaw, B., Burrell, C.L., Gonzalez, S., Taylor, S., 2017. Second-harmonic generation
597 imaging of collagen in ancient bone. Bone Rep. 7, 137–144.
598 https://doi.org/10.1016/j.bonr.2017.10.005
599 Wang, C., Wang, N., Liu, S., Choo-Simth, L.-P., Zhang, H., Zhi, Z., 2018. Investigation of Microfibril
600 Angle of Flax Fibers Using X-Ray Diffraction and Scanning Electron Microscopy. J. Nat. Fibers
601 1–10. https://doi.org/10.1080/15440478.2018.1546639
602 Wardrop, A.B., 1962. Cell wall organization in higher plants I. The primary wall. Bot. Rev 28, 241–285.
603 https://doi.org/10.1007/BF02860816
604 Williams, R.M., Zipfel, W.R., Webb, W.W., 2005. Interpreting Second-Harmonic Generation Images of
605 Collagen I Fibrils. Biophys. J. 88, 1377–1386. https://doi.org/10.1529/biophysj.104.047308
606 Zhao, Y., Takahashi, S., Li, Y., Hien, K.T.T., Matsubara, A., Mizutani, G., Nakamura, Y., 2018.
607 Ungerminated Rice Grains Observed by Femtosecond Pulse Laser Second-Harmonic
608 Generation Microscopy. J. Phys. Chem. B 122, 7855–7861.
609 https://doi.org/10.1021/acs.jpcb.8b04610
610 Zubkovs, V., Jamme, F., Kascakova, S., Chiappini, F., Le Naour, F., Réfrégiers, M., 2014. Single vs. two-
611 photon microscopy for label free intrinsic tissue studies in the UV light region. Anal., 139,
612 2663–2667. https://doi.org/10.1039/C4AN00203B
613

614

615

616

617

618

619 **FIGURES CAPTION**

620

621 **Figure 1.** Schematic representation of the multi-layer structure of a flax fibre with the primary
622 cell wall (P) and secondary cell wall made of the S1, S2 and S3 layers.

623 **Figure 2.** Raw flax fibres (a), single flax fibre glued on paper card for handling and testing (b)
624 and SGH microscope (c).

625 **Figure 3.** Experimental setup of the multiphoton confocal microscope (NIKON, France). The
626 two SHG channels are marked in red.

627 **Figure 4.** Flax fibre with a maize starch grain manually deposed on the surface. It is possible
628 to compare their signals at different polarisation angles. Backward (green) and forward (red)
629 SHG signal combination. Acquisition parameters: 5% laser power and acquisition range of 0-
630 135°, which represent the laser position as a function of the fibre axis. The edges of the fibres
631 are highlighted with a dotted white curve, same fibre was used for the 4 polarization angles.

632 **Figure 5.** Principe of the image analysis workflow for estimating preferred orientation of
633 fibres. (A), (B), (C), (D): Results of morphological openings applied on image (A) using
634 horizontal line structuring with lengths 10, 20 and 40 pixels. The size of the structuring
635 elements is represented in the bottom part of each image. (E), (F), (G), (H): Results of
636 morphological openings using 7-degrees oriented line structuring elements with the same
637 sizes. (I), (J): Mapping of the typical linear size in the direction 0° and 7°, obtained by
638 computing mean size from oriented granulometry curve of each pixel. (K) Profile of the
639 typical linear size depending on the orientation for a sample pixel shown as a black cross in
640 images (I) and (J). For this pixel, the profiles exhibit a peak around 5 degrees. (L) Parametric
641 mapping of the preferred orientation for each pixel. Red colours correspond to preferred
642 horizontal directions.

643 **Figure 6.** Backward (green) and forward (yellow) SHG emission of a flax fibre at 2°.

**Figure 7.** Flax fibres (a) and cotton trichomes (b). The angle θ marked on flax is 7°, while for cotton, it is 28°. Acquisition parameters: 10% laser power, acquisition range of 0-68°, and forward second-harmonic emission. The angle is defined based on the orientation of the fibre axis taken as X-axis.

**Figure 8.** SHG investigations of several flax fibres (a) and different areas of a single flax fibre (b). One can observe the changes in the MFA depending on the zone (red arrows). Acquisition parameters: 5% laser power and forward emission (yellow), 2° HWP.

**Figure 9.** Imaging process by MATLAB with histograms of the relative microfibril angle detected from the Fig.8b. The first histogram (A) is related to the whole fibre (B); the grey arrow indicates the dislocation zone (kink-band). The areas 1, 2 and 3 (D, E and F) are processed separately. The scale of colors according the orientation is shown in (C).

**Figure 10.** a) Cotton trichomes observed at two different polarisation angles (6° and 44°), where two microfibril orientations (Z and S) are observed. Acquisition parameters: 10% laser power, acquisition range of 0-135°, and forward emission (yellow). b) Cotton trichome structure (Bourmaud et al., 2018)**.**

**Figure 11.** Two different flax fibres investigated with different autofluorescence channels (R460/60 and T460/60 TNDD blue-cyan; R550/88 and T550/88 TNDD magenta) combined to highlight their different layers. It is possible to identify the lumen (L) in the middle (b) and two small layers at the edge of the fibre due to the primary cell wall (P) with the S1 layer (a). The thicknesses of the lumen surrounded by the S3 layer and the P+S1 layers (b) were measured with ImageJ software, and the different diameters of the lumen can be due to the different maturities of the fibres analysed.

## TABLE CAPTION

**Table 1.** Some of the most commonly used methods to calculate the microfibrillar angle of flax fibre elements.

**Figure 1.** Schematic representation of the multi-layer structure of a flax fibre with the primary cell wall (P) and secondary cell wall made of the S1, S2 and S3 layers.

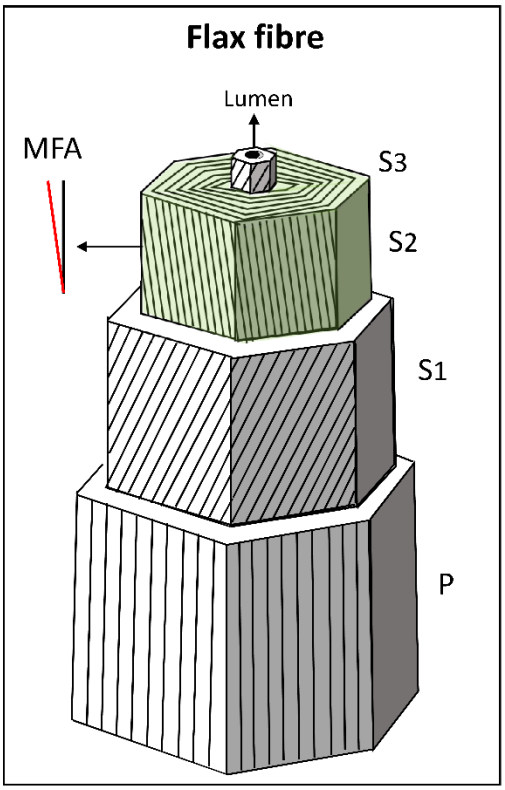


**Figure 2.** Raw flax fibres (a), single falx fibre glued on paper card for handling and testing (b) and SGH microscope (c).

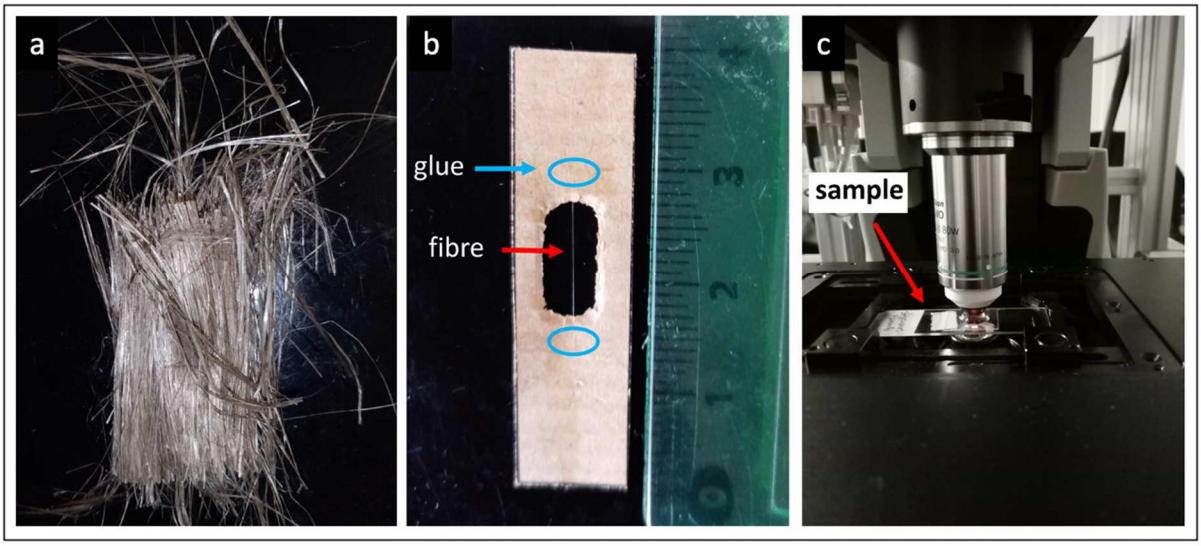

**Figure 3.** Experimental setup of the multiphoton confocal microscope (NIKON, France). The two SHG channels are marked in red.

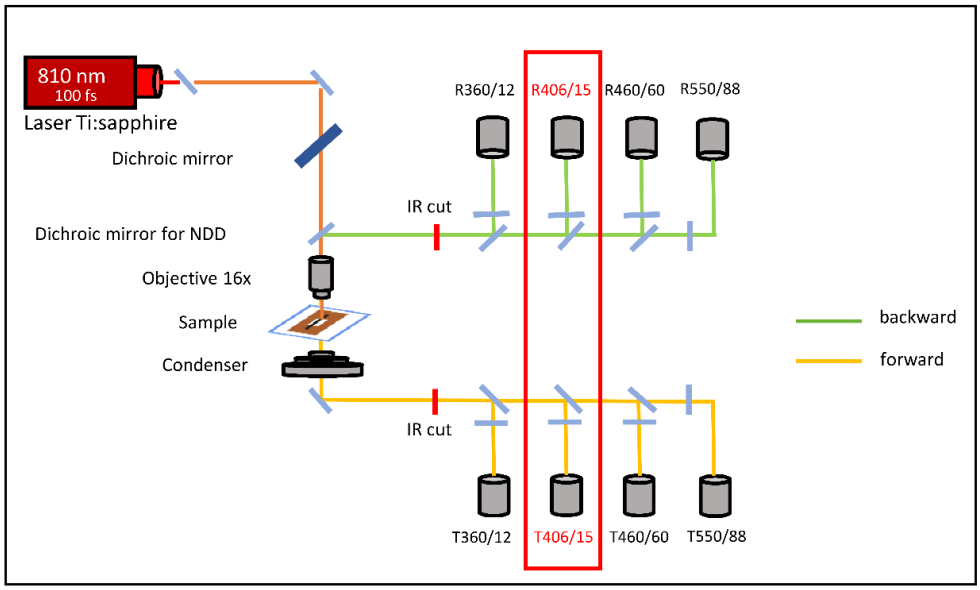


**Figure 4.** Flax fibre with a maize starch grain manually deposed on the surface. It is possible to compare their signals at different polarisation angles. Backward (green) and forward (red) SHG signal combination. Acquisition parameters: 5% laser power and acquisition range of 0-135°, which represent the laser position as a function of the fibre axis. The edges of the fibres are highlighted with a dotted white curve, same fibre was used for the 4 polarization angles.

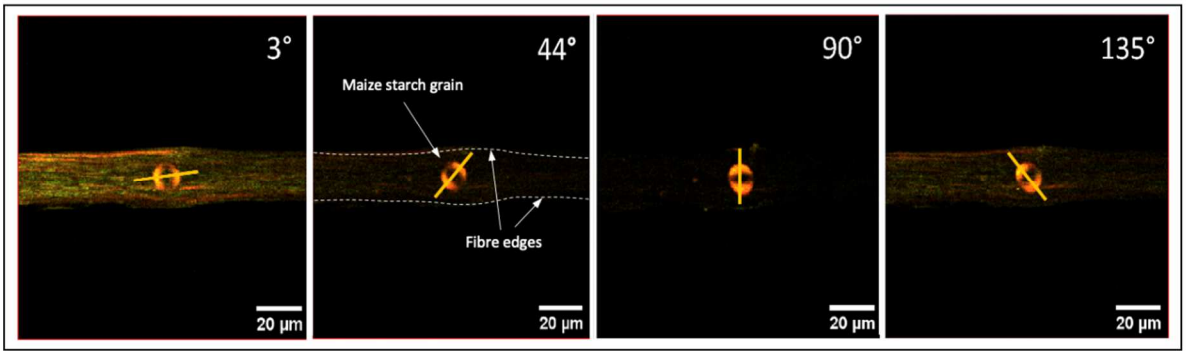

**Figure 5.** Principe of the image analysis workflow for estimating preferred orientation of fibres. (A), (B), (C), (D): Results of morphological openings applied on image (A) using horizontal line structuring with lengths 10, 20 and 40 pixels. The size of the structuring elements is represented in the bottom part of each image. (E), (F), (G), (H): Results of morphological openings using 7-degrees oriented line structuring elements with the same sizes. (I), (J): Mapping of the typical linear size in the direction 0° and 7°, obtained by computing mean size from oriented granulometry curve of each pixel. (K) Profile of the typical linear size depending on the orientation for a sample pixel shown as a black cross in images (I) and (J). For this pixel, the profiles exhibit a peak around 5 degrees. (L) Parametric mapping of the preferred orientation for each pixel. Red colours correspond to preferred horizontal directions.

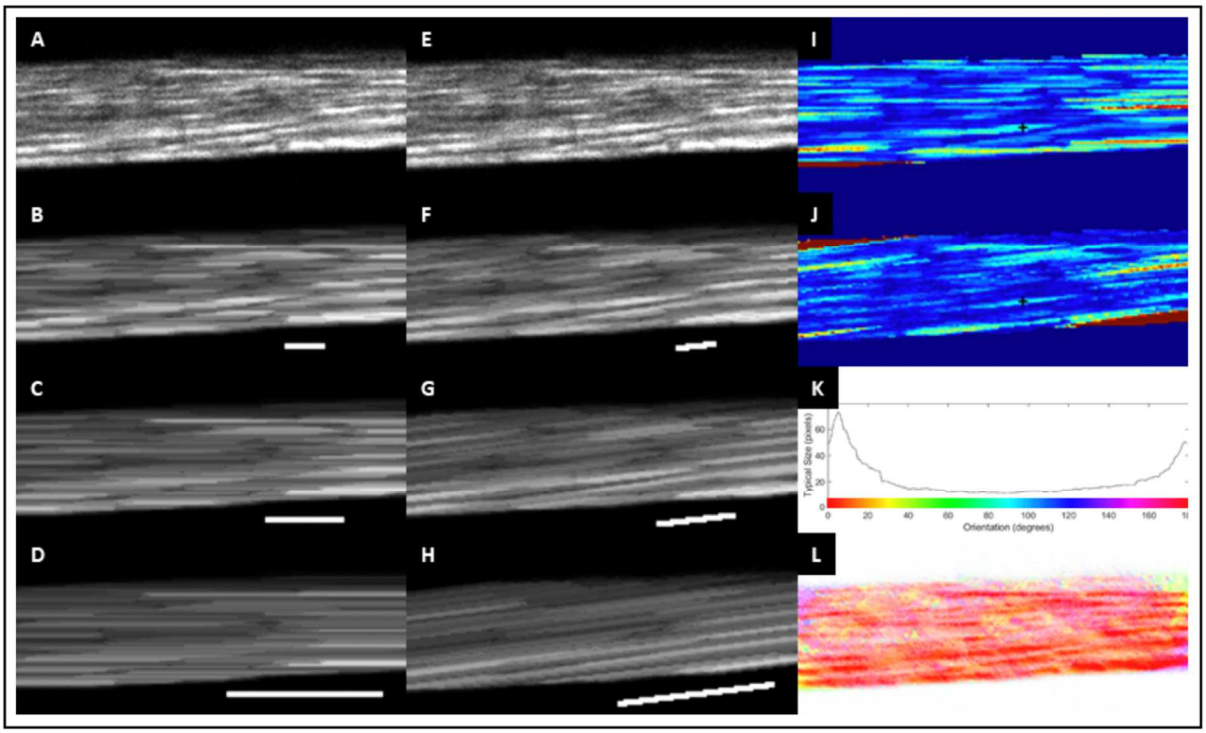

**Figure 6.** Backward (green) and forward (yellow) SHG emission of a flax fibre at 2°.

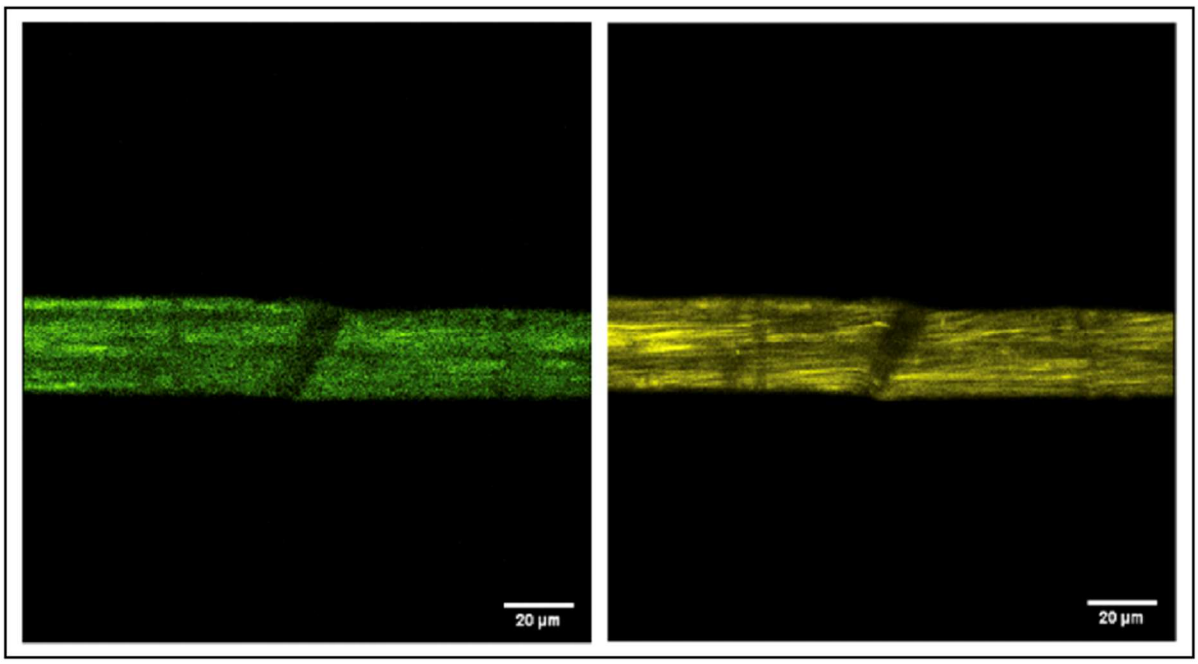


**Figure 7.** Flax fibres (a) and cotton trichomes (b). The angle θ marked on flax is 7°, while for cotton, it is 28°. Acquisition parameters: 10% laser power, acquisition range of 0-68°, and forward second-harmonic emission. The angle is defined based on the orientation of the fibre axis taken as X-axis.

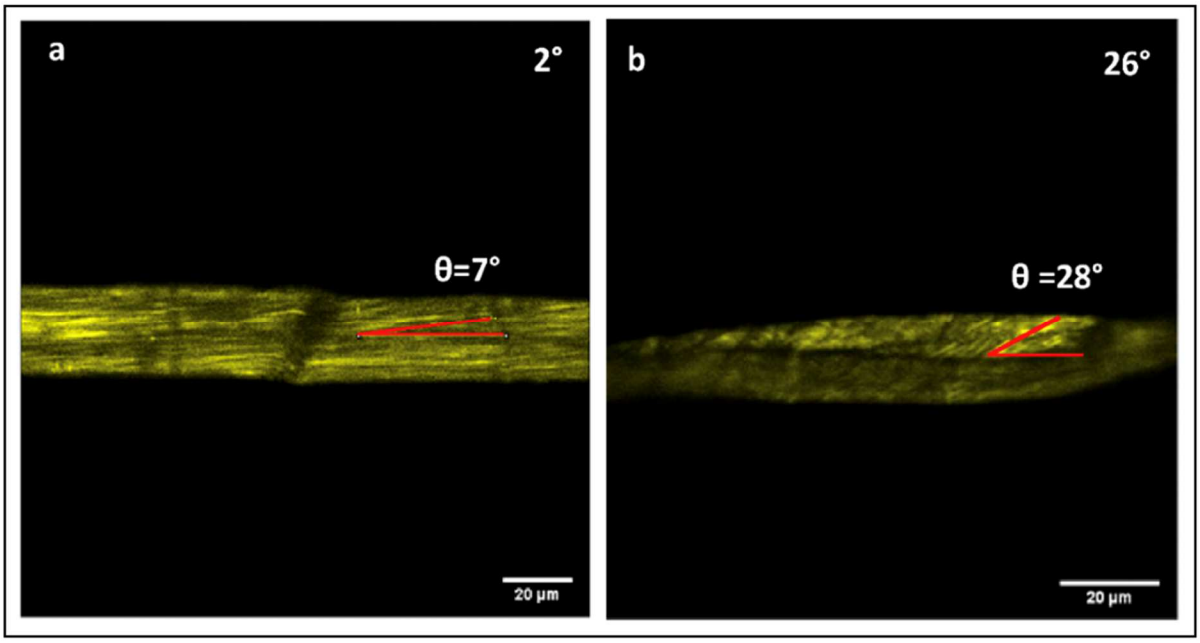

**Figure 8.** SHG investigations of several flax fibres (a) and different areas of a single flax fibre (b). One can observe the changes in the MFA depending on the zone (red arrows). Acquisition parameters: 5% laser power and forward emission (yellow), 2° HWP.

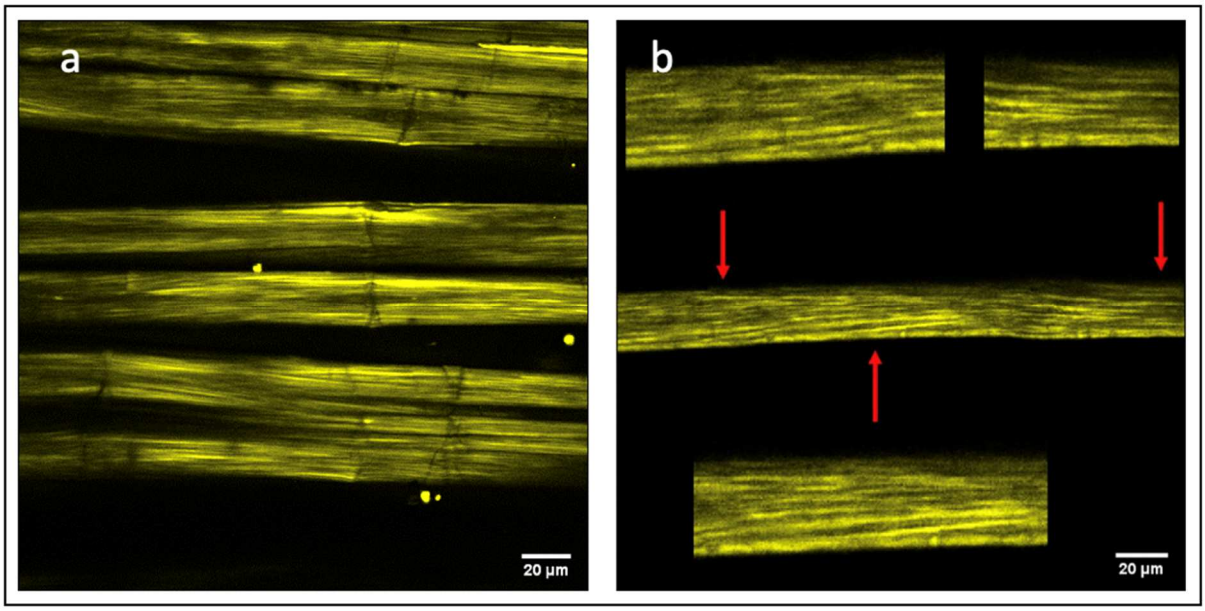

**Figure 9.** Imaging process by MATLAB with histograms of the relative microfibril angle detected from the Fig.7b. The first histogram (A) is related to the whole fibre (B); the grey arrow indicates the dislocation zone (kink-band). The areas 1, 2 and 3 (D, E and F) are processed separately. The scale of colors according the orientation is shown in (C).

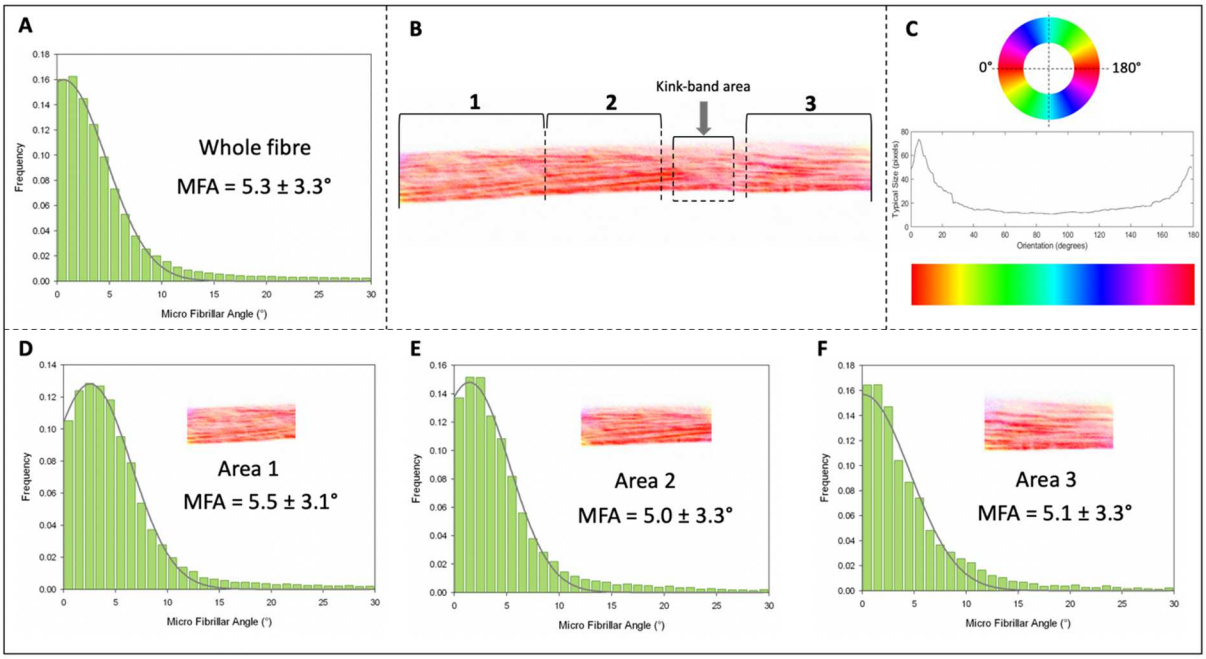

**Figure 10.** a) Cotton trichomes observed at two different polarisation angles (6° and 44°), where two microfibril orientations (Z and S) are observed. Acquisition parameters: 10% laser power, acquisition range of 0-135°, and forward emission (yellow). b) Cotton trichome structure (Bourmaud et al., 2018)**.**

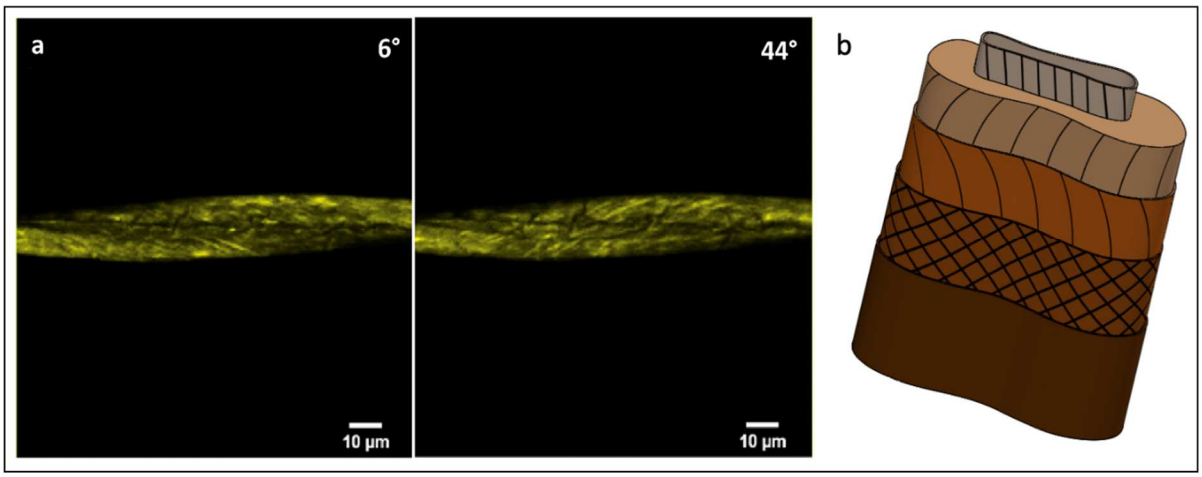

**Figure 11.** Two different flax fibres investigated with different autofluorescence channels (R460/60 and T460/60 TNDD blue-cyan; R550/88 and T550/88 TNDD magenta) combined to highlight their different layers. It is possible to identify the lumen (L) in the middle (b) and two small layers at the edge of the fibre due to the primary cell wall (P) with the S1 layer (a). The thicknesses of the lumen surrounded by the S3 layer and the P+S1 layers (b) were measured with ImageJ software, and the different diameters of the lumen can be due to the different maturities of the fibres analysed.

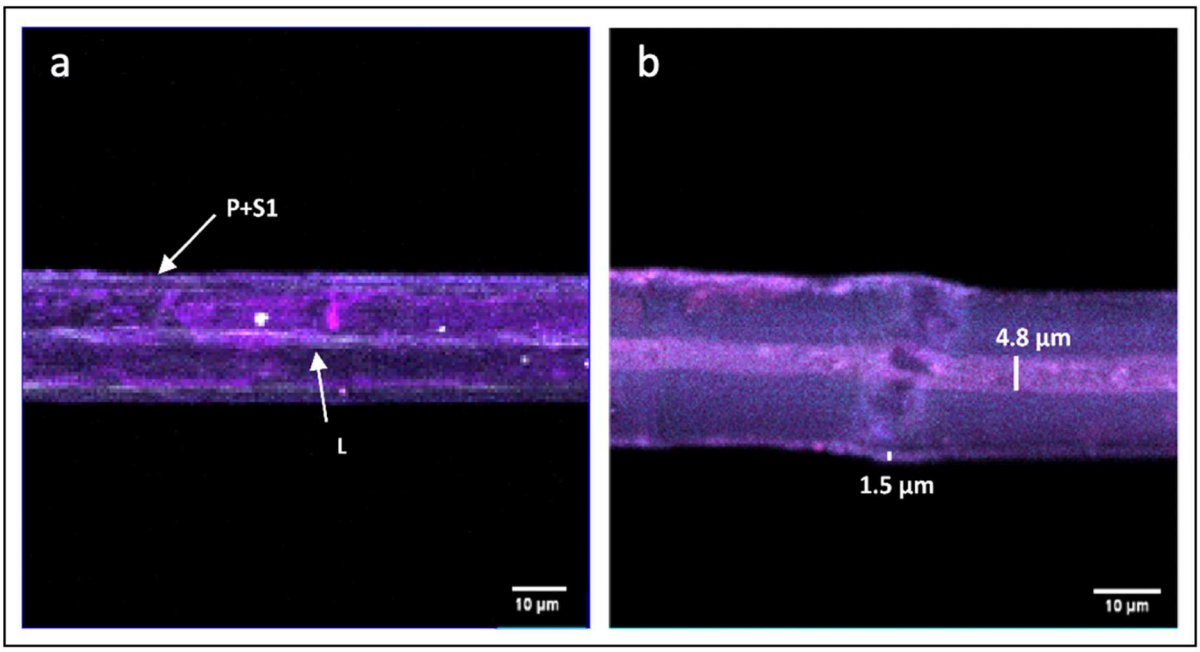

**Table 1.** Some of the most commonly used methods to calculate the microfibrillar angle of flax fibre elements.

| Technique used | MFA of flax fibre | References |
|---|---|---|
| μSAXS | 3.5°-6.4° | (Müller et al., 2000; Muller et al., 1998) |
| SAXS | 11° | (Astley and Donald, 2001) |
| XRD (Cu source) | 6.2°- 9.5° | (Wang et al., 2018; Bourmaud et al., 2013) |
| SEM/ESEM | 5.8°-10° | (Wang et al., 2018; Bos and Donald, 1999) |